Arab J. Nucl. Sci. Appl., Vol. 53, 1, 76-87 (2020)

Arab Journal of Nuclear Sciences and Applications

ISSN 1110-0451 **Web site: ajnsa.journals.ekb.eg** **(ESNSA)**

Radioactivity and Geochemistry of Wadi El Reddah Stream Sediments, North Eastern Desert, Egypt

O. A. Ebyan, H. A. Khamis, H. H. Ali[a], N. S. Abed

[a] *Nuclear Materials Authority (NMA), Cairo, Egypt*

Received 27th Jun. 2019
Accepted 16th Dec. 2019

Wadi El Reddah is a semi closed basin as it has only one outlet at its northern tip while the other parts of the wadi collect flood from the internal tributaries along granites and other rock types. ^{238}U activity concentrations range between 101.24 and 347.96 with an average 214.63 Bq Kg^{-1}, ^{234}U between 89.67 and 308.19 Bq Kg^{-1} with an average of 190.10 Bq Kg^{-1}. ^{232}Th activity concentrations vary between 96.42 and 463.71 Bq Kg^{-1} with 240.46 Bq Kg^{-1} as an average. ^{40}K activity ranges between 1092.71 and 1227.25 Bq Kg^{-1} with an average of 1153.82 Bq Kg^{-1}. ^{235}U activity concentration ranges between 4.66 and 17.38 Bq Kg^{-1} with average of 10.19 Bq Kg^{-1}. Most of stream sediment samples exhibit an increase in SiO_2, $Fe_2O_3^t$, Na_2O, P_2O_5 and K_2O and L.O.I, in addition to a prominent decrease in Al_2O_3, TiO_2, MnO, MgO, CaO. However, trace elements in the studied samples show enrichment in Ni, Cu, Pb, Zn, Cd, Ta, Nb, Zr, Y, Rb, Cs, Ga, Hf, Sn, Th, Tl, U, W, Mo, Bi, As, Be, Li, Sb and Au whereas they are depleted in Co, Sr, V, Ag, Cr and Sc. Zr, Hf and Y are relatively immobile and essentially concentrated in the accessory minerals (zircon and its alteration product branirite, xenotime, thorite and uranothorite). Their REE patterns are well characterized by the M- and W-type tetrad effects. The M- type tetrad effect could be inherited from the surrounding granitic rocks whereas the positive Y anomalies intimately associating with the W-type tetrad effect of REE mainly occur in natural aquatic solutions including seawaters and in some hydrogenous deposits. The presence of the two complementary tetrads may indicate the presence of gold mineralization.

Keywords: *Radioactivity/ Geochemistry/ Stream Sediments/ Wadi El Reddah/ Egypt*

Introduction

The importance of Wadi El Reddah area has notably increased in the last few years after the discovery of secondary uranium mineralization in two sites of the stream sediments filling W. El Reddah as well as two uranium occurrences namely GXXIII and GXXIV in the perthitic leucogranite of G. Gattar which gives a clue of the presence of uranium in that sector of Gattar prospect. This study is focused much more on the northeastern part of G. Gattar batholith which represents W. El Reddah area and its environs.

Tetrad behavior controls REE distributions in geological samples such that REE representing quarter, half, three-quarter, and completely filled 4f shells have increased their stability [1]. Two complementary types of tetrad effects in natural samples have been defined, REEs in solid phase show an M-type tetrad effect, while dissolved REEs, usually show the W-type tetrad effect [2].

Masuda *et al.* reported that the occurrence of the tetrad effect in nature has a significant relation to the history of contact or interaction with water. Tetrad effects in REE patterns are mainly accompanied by processes such as high degrees of

Corresponding author: osama_ishere@hotmail.com
DOI: 10.21608/ajnsa.2019.14126.1224

fractional crystallization, hydrothermal alteration, and mineralization [3]. Expressions of tetrad behavior are found recorded in rare metal granites [4-5]. The tetrad effect becomes more conspicuous with the increase of ligand concentration. The positive deviation of Y/Ho from the chondritic ratio could be a feature of not only the W-type tetrad effect, but also the M-type tetrad effect, since Y with no 4f electrons is not a pseudo-lanthanide that behaves like Ho under aqueous conditions [6]. If the M-type tetrad effect originated from water-solid interaction that resulted in the favorable removal of Ho relative to its neighbors from the solid to liquid phase, Y is probably less soluble in water and favorably hosted in or adsorbed on the solid phase in comparison to Ho. In the present paper, we study the radioactivity and geochemistry of Wadi El Reddah stream sediments, in addition to the interpretation of the presence of two complementary types of tetrad effects and their reasons.

Materials and Methods

Ten stream sediment samples were collected from Wadi El Reddah area (Fig. 1). These samples were prepared for γ-ray spectrometric analyses by HPGe detector system. This detector has a relative efficiency of about 60% of the 3″×3″ NaI (Tl) crystal efficiency, resolution of 1.90 keV and peak/Compton ratio of 69.9:1 at the 1.33 MeV gamma transition of 60Co. It is coupled to conventional electronics connected to a multichannel analyzer card (MCA) installed in a PC computer. The efficiency calibration was performed by using three well-known reference materials obtained from the International Atomic Energy Agency for U, Th and K activity measurements: RGU-1, RGTh-1 and RGK-1 [7-8]. Absolute efficiency calibration of the gamma spectrometry system was carried out using the radionuclide specific efficiency method in order to reduce the uncertainty in gamma-ray intensities, as well as the influence of coincidence summation and self-absorption effects of the emitting gamma photons [9]. Uranium- 238 activity was determined indirectly from the gamma rays emitted by its daughter products (^{234}Th and ^{234m}Pa) whose activities are determined from the 63.3 and 1001 keV photo peaks, respectively [10]. The ^{234}U activity was determined directly from the gamma rays emitted from this nuclide at energies of 53.2 and 120.9 keV [11-12-13]. For the measurement of the ^{230}Th activity, the γ-ray emission values at 67.7 keV is used [14].The specific activity of ^{226}Ra was measured using the 186.1 keV from its own gamma-ray (after the subtraction of the 185.7 keV of ^{235}U). The specific activity of ^{214}Pb was measured using the 241.9, 295.2 keV and 351.9 keV while the specific activities of ^{214}Bi and ^{210}Pb were measured using 609.3 and 46.5 keV, respectively.

Uranium-235 activity was determined directly by its gamma-ray peaks; 143.8, 163.4, 185.7, and 205.3 keV [15-13-16]. The specific activity of ^{232}Th was measured using the 338.4 keV and 911.2 keV from 228Ac and 583 keV and 2614.4 keV from 208 Tl. The specific activity of ^{40}K was measured directly by its own gamma-ray at 1460.8 keV. Chemical analyses of ten stream sediment samples were carried out in ACME analytical Laboratories of Vandcouver, Canada for major oxides, trace and rare earth elements by ICP-emission spectrometry (ICP-ES) and ICP-mass spectrometry (ICP-MS). Detection limits for major oxides and trace elements are 0.001–0.04 wt. % and 0.01–0.5 ppm respectively. The analytical precision, as calculated from replicate analyses, is 0.5% for major elements and varies from 2 to 20 % for trace elements. Figure (1) presents the location of various stream sediment samples collected from Wadi El Reddah area.

Geological Setting

Wadi El Reddah extends in the N-S direction and represents a semi-closed basin as it has only one outlet at its northern tip while the other parts of the wadi collect flood from the internal tributaries along granites and other rock types. The drainage system of Wadi El Reddah reveals the presence of two to three sub-basins along its course. These are the southeastern, central and northeastern sub-basin (Fig. 2). Each of the mentioned sectors collects their streams and floods from different rocks that extend around the semi-circular southern margin of this wadi. This will help too much in prospecting these remote and highly elevated points especially in Gattar granites. W. El Reddah is truncated northward with the main course of W. Bali and is considered as one of its branches and drains to it. Wadi El Reddah is mainly surrounded by scattered exposures in a chronogical sequence of metavolcanics and metagabbro-diorite complex in addition to long sector of Hammamat

sedimentary rocks, monzongranites of G. El Reddah, perthitic leucogranites of G. Gattar as well as swarms of post-granitic dykes (Fig. 2). Wadi El Reddah has a higher ground relative to the ground adjacent to the surrounding peaks. The floor of the Wadis and their tributaries in Gabal Gattar area are generally covered by thick recent Wadi sediments. These sediments are unconsolidated, loose and consist of fluvial sediments formed of sands, pebbles, gravels, cobbles and boulders. Fluvial soils exist largely because of soil creep in area of high relief. The thickness of the stream sediments of the studied area can be estimated from the groundwater wells. It ranges from 25 to 30 meters.

Results

Activity concentrations of ^{238} U, ^{235}U, ^{234}U, ^{230}Th, ^{226}Ra, ^{40}K and isotopic compositions are reported in Table (1) (in Bq/kg and ppm) for the studied stream sediments by HPGe detector. ^{238}U activity concentrations range between 101.24 and 347.96 with an average 214.63 Bq Kg^{-1}, ^{234}U between 89.67 and 308.19 Bq Kg^{-1} with average 190.10 Bq Kg^{-1}. ^{232}Th activity concentrations vary between 96.42 and 463.71 Bq Kg^{-1} with 240.46 Bq Kg^{-1} as an average. ^{40}K ranges between 1092.71 and 1227.25 Bq Kg^{-1} with an average 1153.82 Bq Kg^{-1}. ^{235}U activity concentration ranges between 4.66 and 17.38 Bq Kg^{-1} with average 10.19 Bq Kg^{-1}. The world concentration limits of ^{238}U, ^{232}Th and ^{40}K are 35, 30 and 400 Bq Kg^{-1}, respectively [17]. The studied samples have higher values compared to those reported by the UNSCEAR.

A significant difference of ^{238}U/^{235}U ratios in the studied stream sediments which ranges between 21.52 and 22.24 suggest that redox conditions play an important role in the fractionation of ^{238}U and ^{235}U [18-19]. Theoretically, nuclear-field effects could play a major role in ^{238}U/^{235}U isotope fractionation wherein the heavier isotope is preferentially partitioned into the more reduced species [20-21]. ^{234}U/^{235}U ratios in the studied sediments show a narrow range between 19.06 and 19.87, which means that uranium-235 mobility in most samples with respect to uranium-234 confirming the role of alteration processes by the acidic solutions affecting these sediments.

^{234}U/ ^{238}U and ^{230}Th/^{238}U Activity Rates (ARs) of the studied stream sediments have been measured (from 0.68 to 0.89 and from 0.84 to 1.14, respectively), deviating from the secular equilibrium values, indicating open-system behavior with respect to ^{238}U daughter isotopes within the oxidized zone due to preferential mobilization of ^{234}U relative to ^{238}U from the sediments. The lowered ^{234}U/^{238}U ARs in the studied stream sediments could be the result of the addition of uranium from anomalous Gattar granites with a high uranium concentration and as dissolved uranium. As for ^{234}U/ ^{238}U, the radioactive disequilibria of ^{230}Th/^{234}U are mainly produced by α-decay enhanced dissolution, re-adsorption and re-precipitation of ^{234}U.^{226}Ra/^{238}U and ^{226}Ra/^{230}Th activity ratios are nearly less than1 in all samples, indicating that U and Th fixing is the main process responsible for lowering these ratios. The activity ratios of ^{234}U/ ^{238}U, ^{230}Th/ ^{234}U and ^{226}Ra/ ^{230}Th for the studied sediments show obvious deviations from secular equilibrium, indicating the presence of water–rock interactions during the last 1 Ma and probably longer [22-23].

Geochemistry of major and trace elements in the studied stream sediments:

The results of major, trace and REEs for Wadi El Reddah stream sediments are given in Table (2). Geochemically, the variations of major and trace elements could be attributed to the loss and gain of elements. To understand the geochemical behavior of major and trace elements in the studied stream sediments, it is recommended to normalize these sediments to the upper continental crust (UCC) referred to by Rudnick et al.[24]. After that, the reference UCC becomes flat at unity and the relative depletion or enrichment is given by the deviations on both sides of the reference line (Figs. 3 & 4). The geochemistry of major elements is discussed in terms of gains (positive) and losses (negative) of these elements during stream sediment formation from the mother rocks. Most of stream sediment samples exhibit an increase in SiO_2, $Fe_2O_3^t$, Na_2O, P_2O_5 and K_2O and L.O.I., a prominent decrease in Al_2O_3, TiO_2, MnO, MgO, CaO (Fig. 3). The enrichment of Na_2O and K_2O are manifested by the presence of feldspars. The increase in SiO_2 may be related to the desilicification of the surrounding granites and migration of silica to these sediments. The enrichment of Fe_2O may be due to hematitization. P_2O_5 increased in the sediments, reflecting that apatite continued to form during granitic rock alteration and sedimentation processes.Formation of titanite is reflected by increased TiO_2 contents.

However, trace elements in the studied samples show enrichment in Ni, Cu, Pb, Zn, Cd, Ta, Nb, Zr, Y,Rb, Cs, Ga, Hf, Sn, Th, Tl, U, W, Mo, Bi, As, Be, Li, Sb and Au, whereas they are depleted in Co, Sr, V, Ag, Cr and Sc **Fig. (4)**. Pb concentration increases as a result of the alteration of Pb minerals from the surrounding granites including kasolite, cotunite, coronadite and galena. Zr, Hf and Y are relatively immobile and essentially concentrated in the accessory minerals (zircon and its alteration product branirite, xenotime, thorite and uranothorite). High contents of U, Th, Y, Nb and Ta may be related to the presence of fergsunite (Y, RE) NbO_4), xenotime Y (HRE) (PO_4), ferrocolumbite, yttrocolumbite, columbite and monazite (Ce, La, Nd, Th) PO_4 as indicated from the mineralogical studies.

Fig. (1): Land sat image showing the sampling sites along wadi El Reddah

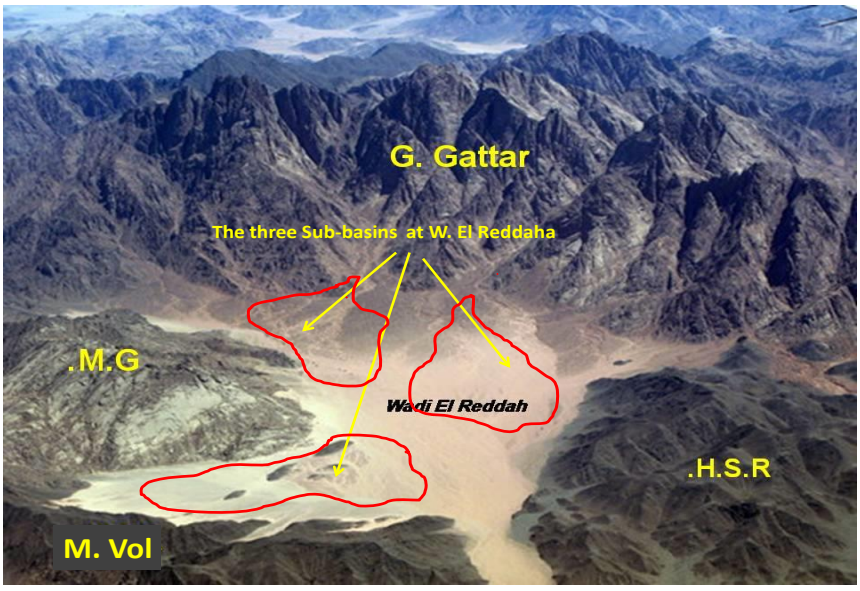

Fig. (2): Wadi El Reddah and its course subdivisions and the exposed rock types (where H.S.R. is Hammamat sedimentary rocks

M. Vol. is metavolcanics and M.G. is monzogranite of gabal El Reddah)

Table (1): radionuclide activity concentrations and their activity ratios of El Reddah stream sediments

Nuclide	Wr-10	4-2	12-1	14-2	Nv-1	Min	Max	Average
^{238}U series								
^{234}Pa	**346.28**	**342.49**	**167.37**	**112.64**	**99.52**	**99.52**	**346.28**	**213.66**
^{234}U	**306.44**	**308.19**	**146.42**	**99.78**	**89.67**	**89.67**	**308.19**	**190.10**
^{230}Th	**349.47**	**335.20**	**138.53**	**114.57**	**111.20**	**111.20**	**349.47**	**209.79**
^{226}Ra	**335.10**	**239.14**	**141.61**	**100.64**	**101.93**	**100.64**	**335.10**	**183.68**
^{214}Pb	**308.32**	**230.10**	**136.57**	**94.05**	**91.53**	**91.53**	**308.32**	**172.11**
^{214}Bi	**309.70**	**230.42**	**136.74**	**93.84**	**93.81**	**93.81**	**309.70**	**172.90**
^{210}Pb	**246.13**	**208.08**	**138.19**	**94.25**	**86.34**	**86.34**	**246.13**	**154.60**
^{238}U	**345.98**	**347.96**	**165.31**	**112.66**	**101.24**	**101.24**	**347.96**	**183.10**
^{232}Th series								
^{228}Ac	**465.05**	**396.13**	**147.63**	**96.33**	**97.26**	**96.33**	**465.05**	**240.48**
^{208}Tl	**457.23**	**389.24**	**145.65**	**94.55**	**95.21**	**94.55**	**457.23**	**236.38**
^{232}Th	**463.71**	**395.31**	**148.56**	**96.42**	**98.29**	**96.42**	**463.71**	**240.46**
^{235}U	**15.42**	**17.38**	**7.68**	**5.81**	**4.66**	**4.66**	**17.38**	**10.19**
^{40}K	**1200.91**	**1092.71**	**1227.25**	**1100.95**	**1147.30**	**1092.71**	**1227.25**	**1153.82**
^{238}U/^{235}U	**22.44**	**21.72**	**21.52**	**21.63**	**21.74**	**21.52**	**22.44**	**21.81**
^{234}U/^{235}U	**19.87**	**19.23**	**19.06**	**19.16**	**19.26**	**19.06**	**19.87**	**19.32**
^{234}U/ ^{238}U	**0.68**	**0.886**	**0.886**	**0.787**	**0.885**	**0.68**	**0.89**	**0.82**
^{226}Ra/ ^{238}U	**0.97**	**0.69**	**0.86**	**0.89**	**1.01**	**0.69**	**1.01**	**0.88**
^{230}Th/ ^{238}U	**1.01**	**1.14**	**0.84**	**1.02**	**1.10**	**0.84**	**1.14**	**1.02**
^{230}Th/ ^{234}U	**0.94**	**0.94**	**0.95**	**1.15**	**1.24**	**0.94**	**1.24**	**1.04**
^{226}Ra/ ^{230}Th	**0.96**	**0.71**	**1.02**	**0.88**	**0.92**	**0.71**	**1.02**	**0.90**
^{210}Pb/ ^{226}Ra	**0.73**	**0.87**	**0.98**	**0.94**	**0.85**	**0.73**	**0.98**	**0.87**
U (ppm)	**27.93**	**18.33**	**13.33**	**9.09**	**8.16**	**8.16**	**27.93**	**15.37**
Th (ppm)	**114.78**	**97.85**	**36.77**	**23.87**	**24.33**	**23.87**	**114.78**	**59.52**
K (%)	**3.84**	**3.49**	**3.92**	**3.52**	**3.67**	**3.49**	**3.92**	**3.69**
Th/U	**4.11**	**5.34**	**2.76**	**2.63**	**2.98**	**2.63**	**5.34**	**3.56**

The reasons of W-type tetrad effect in the stream sediments at W. El Reddah

ΣREE mean concentration is 636.52 ppm. Non-chondritic yttrium/holmium ratio and lanthanide tetrad effect were observed in the studied sediments. Average UCC-normalized ratios of REEs in El Reddah sediments indicate that there is apparently an enrichment of HREE with respect to LREE (La/Yb)UCC = 0). Europium anomalies are also present in the studied sediments ([Eu/Eu*] =0.2 to 0.5, average=0.4).

Y/Ho ratios for the studied sediments show large positive deviations from the chondritic ratio. Similar non-chondritic Y/Ho ratios are seen in a Precambrian limestone from South Africa, seawaters, and marine phosphorites. Their REE patterns are well characterized by the M- and W-type tetrad effects (**Fig. 5 and Table 2**). The M-type tetrad effect is inherited from the surrounding granitic rocks whereas the positive Y anomalies intimately associated with the W-type tetrad effect

of REE mainly occur in natural aquatic solutions including seawaters and in some hydrogenous deposits. The presence of the two complementary tetrads may indicate the presence of gold mineralization **[25]**. This can be improved by gold concentration measured by Fire assay in one of these samples that reach up to 0.7 ppm. Also, gold is confirmed mineralogically by separation of minerals by bromoform and picking of gold-bearing minerals. Gold bearing minerals were analysed by EDAX using ESEM. Gold is recorded in sulphide minerals (chalcopyrite), which associated with invisible gold. The presence of gold in chalcopyrite has concentration reach up to 1.62 wt%. (**Fig. 6**).

Referring to the geological history of the region, it is very important to mention that the Gattar-Dokhan area is considered as the rift-shoulder during the time of the Red sea Rifting tectonics. In addition, Esh El mallaha Range was considered as a high up-lifted or tectonically raised elongated block or island within the Miocene Red sea paleo-shore line. When mapping the area of the Red sea coast between 27° 00' – 27° 10'N, several scattered Eocene and Miocene exposures are recorded along the Red sea coast, between Esh El mallaha and the Red sea hills and even near the Red sea hills. The nearest exposure of the Eocene- Miocene succession is located 7Km away from the entrance of W. El Reddah (the studied area). This may give a clue about the location of the shoreline and basin depocentre. The presence of these exposures of miocene carbonates and evaporates near and close to the basement (close to G. Salat Bali) indicates that the sea water invades and cover most of the promontraiy areas of the basement and may extend through the main engulfed wadies like W. Bali and W. El Reddah **[26]**. This may clarify the presence of the unusual Y/Ho ratios and w-type tetrad in the studied sediments rare earth pattern.

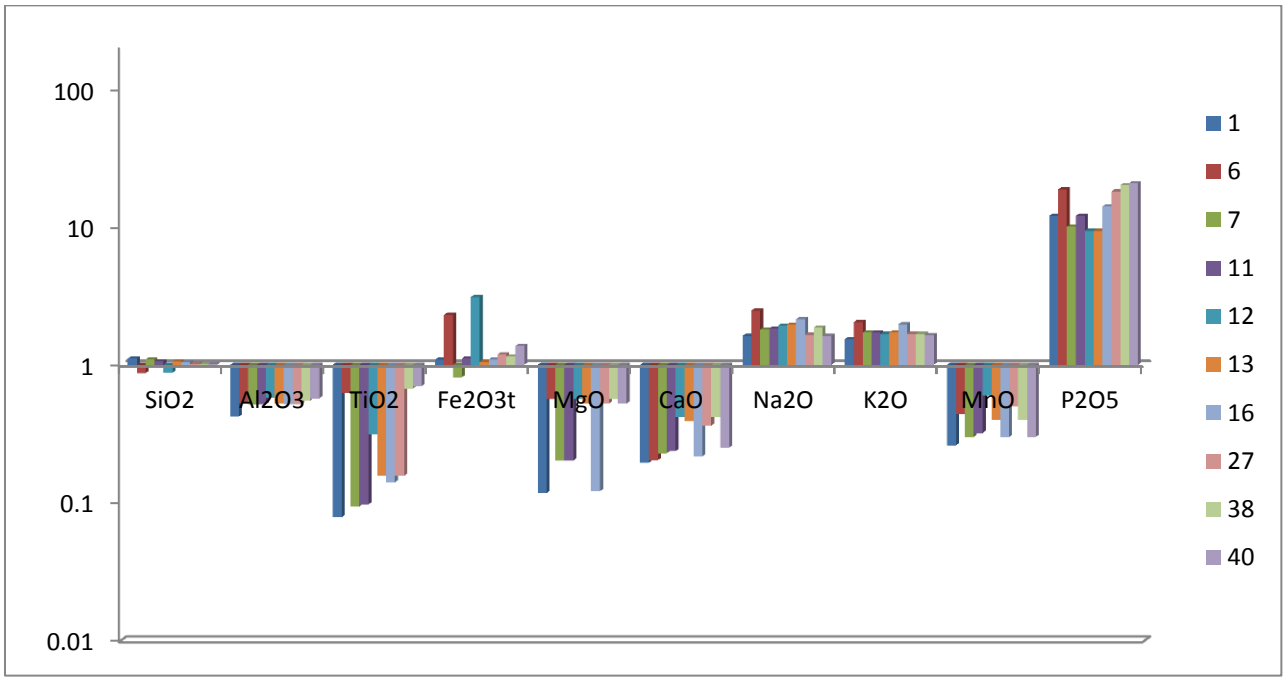

Fig. (3): Concentrations of major oxides of the stream sediments samples normalized to those of UCC as given by [24].

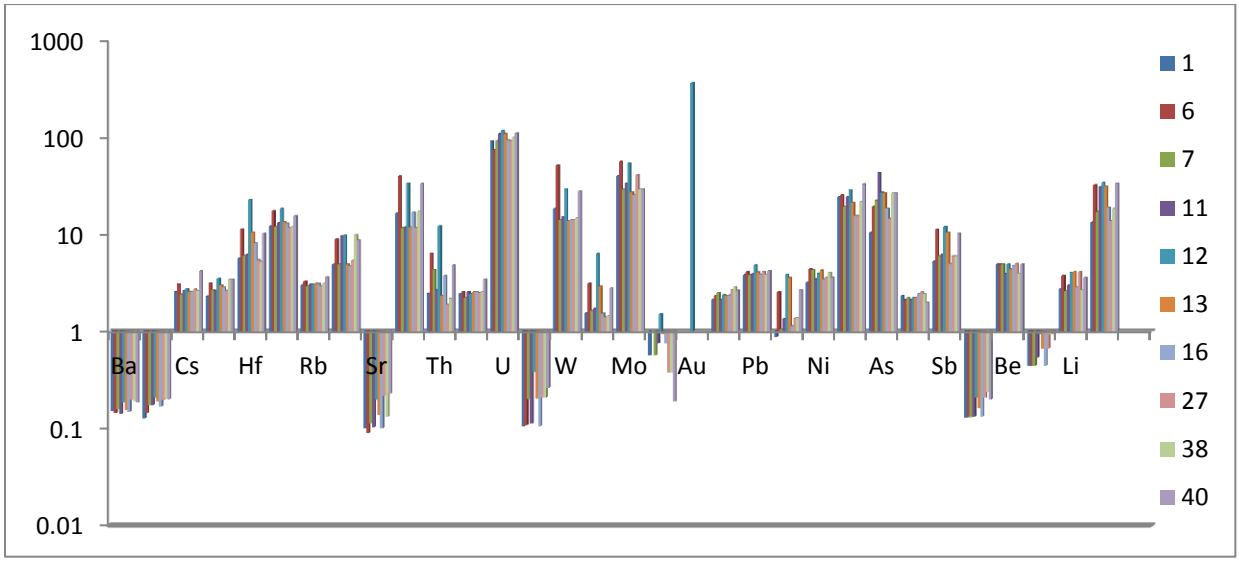

Fig. (4): Concentrations of trace elements of the stream sediments samples normalized to those of UCC as given by [24]

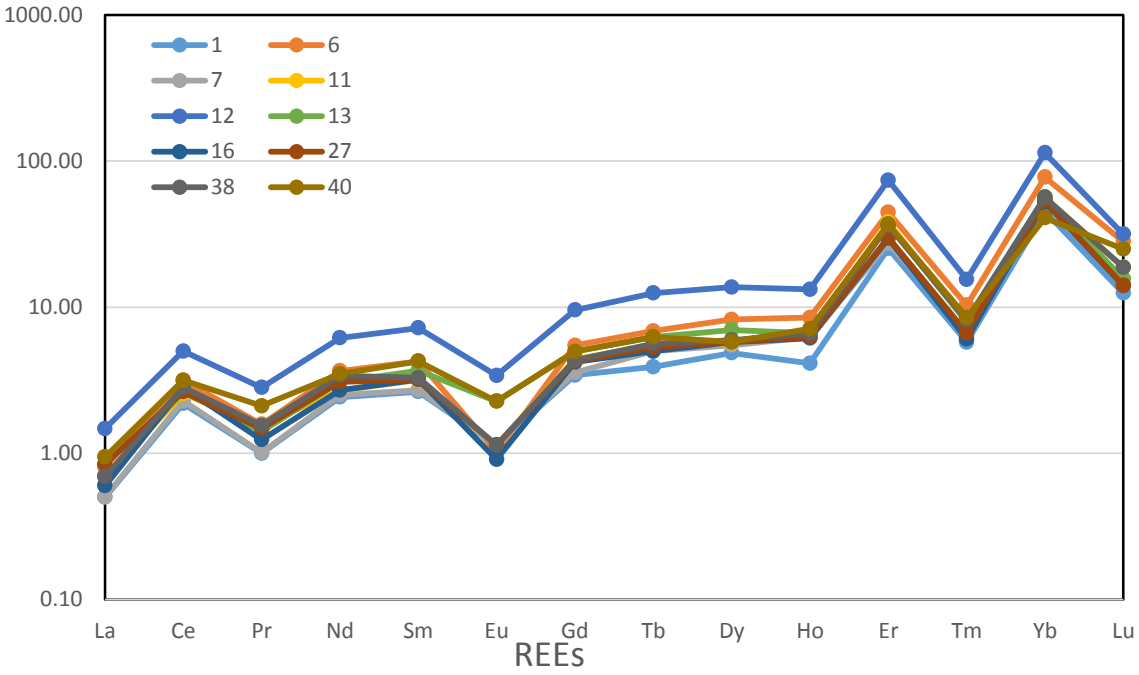

Fig. (5): UCC- normalized REE diagram [27] for the studied stream sediments

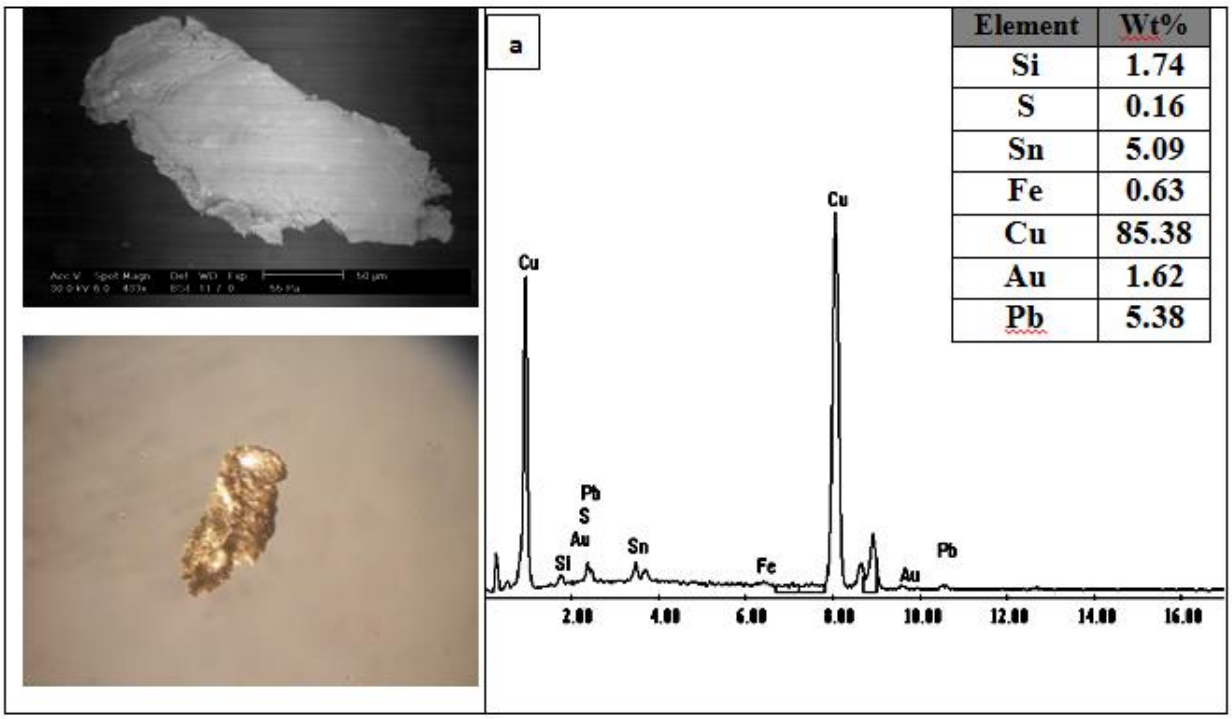

Fig. (6): BSE images and EDX analyses of cupper crystal contains gold as inclusion in stream sediments of Wadi El-Reddah

Table (2): Chemical composition of the Wadi El Reddah stream sediments, Eastern Desert, Egypt

Oxides	Stream Sediments									
%	1	6	7	11	12	13	16	27	38	40
SiO_2	73.96	57.94	72.8	70.8	58.3	70.4	69.6	67.8	67.07	67.2
Al_2O_3	6.5	8.08	7.9	8.0	8.9	8.1	8.0	8.0	8.5	8.8
TiO_2	0.05	0.4	0.06	0.062	0.2	0.1	0.09	0.1	0.43	0.45
$Fe_2O_3^t$	5.5	11.6	4.1	5.6	15.6	5.3	5.5	6.0	5.8	6.9
MgO	0.29	1.4	0.5	0.5	1.4	1.3	0.3	1.3	1.4	1.3
CaO	0.70	0.73	0.82	0.85	1.5	1.4	0.78	1.3	1.5	0.9
Na_2O	5.3	8.08	5.9	6.0	6.3	6.4	7.0	5.4	6.1	5.3
K_2O	4.3	5.71	4.8	4.8	4.7	4.8	5.5	4.7	4.7	4.6
MnO	0.026	0.044	0.03	0.032	0.06	0.04	0.03	0.05	0.04	0.03
P_2O_5	1.8	2.79	1.5	1.8	1.4	1.4	2.1	2.7	3.0	3.1
L.O.I.	0.6	0.6	0.59	0.5	0.7	0.6	0.5	0.7	0.5	0.6
Ba	95	90	98	88	115	97	93	125	120	115
Co	2.2	2.5	3.0	3.0	3.6	3.3	2.9	3.4	3.5	3.45
Cs	12.6	15.1	11.80	12.9	13.4	12.6	12.6	13.3	12.9	20.5
Ga	40.3	55	46.87	46.1	61	52.1	50.3	46.1	60	59.8
Hf	30	60	32	33	121.5	56	43	29	27.8	54
Nb	146.1	210.3	144.2	158.1	222.4	160.8	156.3	140.3	143.8	187
Rb	250.8	273.6	246.8	255.2	257.7	261.7	260.4	246.5	261.7	305.2
Sn	10.3	18.9	10.3	20.3	20.6	10.3	9.9	11.3	20.8	18.3
Sr	31.9	28.7	36.3	33.1	63	44.3	31.9	69	42.3	73
Ta	14.9	35.9	10.5	10.7	30.3	10.7	15.2	10.5	15.5	30.1
Th	25.8	66.9	45.5	28.3	128	24.6	39.2	20.0	23.0	50.4
Tl	2.2	2.3	2.0	2.3	2.2	2.3	2.29	2.24	2.3	3.1
U	249	202	250	296	320	294	255	250	270	300
V	10.2	10.5	19.5	10.9	37	19.7	10.2	20.1	20.1	25.3
W	35	98	26.8	28.9	56	26.1	26.8	27	28	53
Zr	300.1	600.5	315.45	330.5	1215	560	295.05	270.1	278	540
Mo	44	62	32	37	60	30	28	45	32	32.4
Ag	0.03	-	0.03	0.04	0.08	0.05	0.04	0.02	0.02	0.01
Au	-	-	-	-	-	-	-	-	-	0.73
Cu	59.4	65	70	59.3	67	65.55	66	75	80	74
Pb	64.8	69.7	64.85	66.3	81.5	69.3	65.91	70.5	65.3	72
Zn	59	171.5	70.2	90.5	259	239	76.15	91.5	92.3	180.3
Ni	150	208	202.1	163	186.4	200.5	163	170.3	190.3	170.3
Bi	3.9	4.1	3.1	3.9	4.6	3.4	2.5	2.5	3.5	5.3
As	50	93	108	208	130	128	89	70	128	128
Cd	0.21	0.19	0.2	0.19	0.2	0.2	0.22	0.23	0.22	0.18
Sb	2.1	4.5	2.4	2.5	4.8	4.2	2.0	2.4	2.4	4.1
Cr	11.8	12	12	12.2	19	15	12.2	19	22	18.3
Be	10.3	10.3	10.3	8.3	10.3	9.2	10	10.5	8.3	10.3
Sc	6.2	6.2	6.2	7.5	13.1	9.3	6.2	9.3	13	13.1
Li	57.3	79	55	63	85.2	86.3	60	86	56	75.3
In	0.08	0.09	0.09	0.1	0.2	0.1	0.05	0.15	0.08	0.2
Re	0.02	0.02	0.02	0.02	0.03	0.02	0.02	0.02	0.02	0.02
Y	280	680	360	650	720	660	400	290	390	710
La	15	24.2	15.1	20.5	44.2	20.9	18	25.3	20.8	28.3
Ce	140.3	202.3	146.3	163.9	320	168.6	180.1	169	180.9	202
Pr	7.1	11.2	7.2	11.1	20	10	8.8	10.51	11.01	14.98
Nd	63.1	95.4	65.2	82.1	160.2	80.3	70.3	80.3	88.3	90.9
Sm	11.9	19.2	12.2	14.3	32.4	16.6	14.4	14.4	14.8	19.2
Eu	1	0.9	1	1	3	2	0.8	1	1	2
Gd	13.0	20.8	13.6	16.8	36.3	18.9	16.0	16.2	16.5	18.9
Tb	2.5	4.4	3.2	3.5	8	4	3.2	3.4	3.6	4
Dy	17.0	28.8	19.2	19.8	48	24.5	20.2	20.2	20.8	20.3
Ho	3.3	6.8	5	5.3	10.6	5.3	4.9	5	5.3	5.7
Er	58	102.3	63	88	170	85	68	69	83	85

Tm	**1.9**	**3.4**	**2.2**	**2.6**	**5.1**	**2.6**	**2**	**2.2**	**2.7**	**2.8**
Yb	**100**	**170.5**	**118**	**124**	**250**	**125**	**115**	**118**	**124**	**90**
Lu	**4**	**9**	**4.5**	**6**	**10.1**	**5**	**4.5**	**4.5**	**6**	**8**
La/Yb_n	0.0	0.0	0.0	0.0	0.0	0.0	0.0	0.0	0.0	0.0
La/Sm_n	0.2	0.3	0.4	0.3	0.3	0.3	0.3	0.3	0.3	0.3
Gd/Yb_n	0.1	1.1	1.0	0.9	1.1	1.1	1.0	1.0	1.0	0.9
Sr/Eu	**31.9**	**31.9**	**36.3**	**33.1**	**21.0**	**22.2**	**39.9**	**69.0**	**42.3**	**36.5**
Eu/Sm	**0.08**	**0.05**	**0.08**	**0.07**	**0.09**	**0.12**	**0.06**	**0.07**	**0.07**	**0.10**
Y/Ho	**84.85**	**100.00**	**72.00**	**122.64**	**67.92**	**124.53**	**81.63**	**58.00**	**73.58**	**124.56**
Er/Ho	**17.58**	**15.04**	**12.60**	**16.60**	**16.04**	**16.04**	**13.88**	**13.80**	**15.66**	**14.91**
REE	**438.1**	**699.2**	**475.7**	**546.65**	**1117.9**	**568.7**	**526.2**	**539.01**	**578.71**	**592.0**
LREE	**238.4**	**353.2**	**247**	**280.65**	**579.8**	**298.4**	**292.4**	**300.51**	**316.81**	**357.38**
HREE	**199.7**	**346**	**228.7**	**266**	**538.1**	**270.3**	**233.8**	**238.5**	**261.9**	**234.7**
LREE/HREE	**1.2**	**1.0**	**1.1**	**1.1**	**1.1**	**1.1**	**1.3**	**1.3**	**1.2**	**1.5**
Ce/Ce*	**2.59**	**2.37**	**2.66**	**2.25**	**2.11**	**2.30**	**2.84**	**2.03**	**2.40**	**2.16**
Eu/Eu*	**0.1**	**0.0**	**0.1**	**0.1**	**0.1**	**0.1**	**0.1**	**0.1**	**0.1**	**0.1**
Zr/Hf	**10.00**	**10.01**	**9.86**	**10.02**	**10.00**	**10.00**	**6.86**	**9.31**	**10.00**	**10.00**
Nb/Ta	**9.81**	**5.86**	**13.73**	**14.78**	**7.34**	**15.03**	**10.28**	**13.36**	**9.28**	**6.21**
U/Th	**9.65**	**3.02**	**5.49**	**10.46**	**2.50**	**11.95**	**6.51**	**12.50**	**11.74**	**5.95**
Ba/Sr	**2.98**	**3.14**	**2.70**	**2.66**	**1.83**	**2.19**	**2.92**	**1.81**	**2.84**	**1.58**
Ba/Rb	**0.38**	**0.33**	**0.40**	**0.34**	**0.45**	**0.37**	**0.36**	**0.51**	**0.46**	**0.38**
Rb/Sr	**7.86**	**9.53**	**6.80**	**7.71**	**4.09**	**5.91**	**8.16**	**3.57**	**6.19**	**4.18**
t1	**1.34**	**1.30**	**1.36**	**1.47**	**1.25**	**1.31**	**1.47**	**1.73**	**1.97**	**3.65**
t3	**1.16**	**1.10**	**1.11**	**1.03**	**1.16**	**1.15**	**1.06**	**1.07**	**1.08**	**1.01**
$TE_{1..3}$	**1.25**	**1.20**	**1.23**	**1.40**	**1.20**	**1.23**	**1.25**	**1.15**	**1.21**	**1.99**

t1, t3, t4 and t are calculated according to a previous study **[28]**

- : not determined.

Conclusion

High contents of U, Th, Y, Nb and Ta may be related to the presence of fergsunite $(Y,RE)NbO_4$), xenotime Y(HRE) (PO_4), ferrocolumbite, Yttrocolumbite, columbite and monazite (Ce, La, Nd, Th) PO_4 as indicated from the mineralogical studies. $^{234}U/^{238}U$ and $^{230}Th/^{238}U$ ARs of the studied stream sediments deviate from the secular equilibrium values, indicating the open-system behavior with respect to ^{238}U daughter isotopes within the oxidized zone due to preferential mobilization of ^{234}U relative to ^{238}U from the sediments. The lowered $^{234}U/^{238}U$ ARs in the studied stream sediments can be resulting from the addition of uranium from anomalous Gattar granites with a high uranium concentration and as dissolved uranium. Most of stream sediment samples exhibit increase in SiO_2, $Fe_2O_3^t$, Na_2O, P_2O_5 and K_2O and L.O.I., a prominent decrease in Al_2O_3, TiO_2, MnO, MgO, CaO. However, trace elements in the studied samples show enrichment in Ni, Cu, Pb, Zn, Cd, Ta, Nb, Zr, Y, Rb, Cs, Ga, Hf, Sn, Th, Tl, U, W, Mo, Bi, As, Be, Li, Sb and Au whereas they are depleted in Co, Sr, V, Ag, Cr and Sc. Co-occurrence of tetrad-effects of W- and M-shape in the third and fourth tetrads is observed in the chondrite-normalized REE distribution patterns of Wadi El Reddah stream sediments. The co-existence of W- and M-shape tetrad-effects in Wadi El Reddah stream sediments confirm the idea that penetration of low-pH surface waters into upper part of these sediments might have caused destruction of REE-bearing minerals, leaching and transportation of REE downward, and ultimately their concentration in the lower part probably with the contact with the underlying basement rocks which make as a buffer. The presence of the two complementary tetrads may indicate the presence of gold mineralization. Y/Ho ratios for the studied sediments show large positive deviations from the chondritic ratio and these phenomena with conjugated tetrad mainly occur in natural aquatic solutions including seawaters and in some hydrogenous deposits. This may indicate the probable mixing of acidic surficial water with alkaline sea water during mineralization processes.

REFERENCES

1 McLennan, S.M., and Taylor, S.R., (1979): Rare earth elements mobility associated with uranium mineralization..*J. Nature* ,282, 247–250.

2 Masuda, A., Kawakami, O., Dohomoto, Y., Takenaka, T. (1987): Lanthanide tetrad effects in

nature: two mutually opposite types, W and M. *J. Geochem*, 21, 119–124.

3 Jahn, B., Wu, F., Capdevila, R., Martineau, F., Zhao, Z. and Wang, Y. (2001): highly evolved juvenile granites with tetrad REE patterns: the Woduhe and Baerzhe granites from the Great Xing'an Mountains in NE China. Lithos. 59, 171-198.

4 Monecke T, Kempe U, Monecke J, Sala M, Wolf D. (2002): Tetrad effect in rare earth element distribution patterns: a method of quantification with application to rock and mineral samples from granite-related rare metal deposits. *J. Geochim Cosmochim Acta*, 66,1185–1196.

5 Zhao, Z.-H., Bao, Z.-W., Qiao, Y.-L. (2010): A peculiar composite M- and W-type REE tetrad effect: evidence from the Shuiquangou alkaline syenite complex, Hebei Province, China. *J. Chin. Sci. Bull*, 55, 2684–2696.

6 Kawabe I., Ohta, A., and Miura, N. (1999): Distribution coefficient of REE between Fe oxyhydroxide precipitates and NaCl solutions affected by REE carbonate complexation. *J. Geochem*, 33: 161-197.

7 IAEA, International Atomic Energy Agency 1987. "Preparation and Certification of IAEA Gamma Spectrometry Reference Materials, RGU-1, RGTh-1 and RGK-1". International Atomic Energy Agency. Report-IAEA/RL/148.

8 Anjos, R.M., Veiga, R., Soares, T., Santos, A.M.A., Aguiar, J.G., Frascá, M.H.B.O., Brage, J.A.P., Uzêda, D., Mangia, L., Facure, A., Mosquera, B., Carvalho, C., Gomes, P.R.S., (2005): "Natural Radionuclide Distribution in Brazilian Commercial Granites". *J. Radiation Measurements*, 39, 245–253.

9 Stoulos, S., Manolopoulou, M., Papastefanou, C. (2003): "Assessment of natural radiation exposure and radon exhalation from building materials in Greece". *J. Environ. Radioact*, 69, 225–240.

10 Sutherland, R.A., de Jong, E. (1990): "Statistical Analysis of Gamma-Emitting Radionuclide Concentrations for Three Fields in Southern Saskatchewan, Canada". *J. Health Physics*,58 (4), 417–428.

11 Yokoyama, Y., Falguères, C., Sémah, F., Jacob, T. and Grün, R. (2008): Gamma-Ray Spectrometric Dating of Late Homo Erectus Skulls from Ngandong and Sambungmacan, Central Java, Indonesia. *J. Human Evolution*, 55, 274–277.

12 Yücel, H., Solmaz, A.N., Köse, E. and Bor, D. (2010) Methods for Spectral Interference Corrections for Direct Measurements of 234U and 230Th in Materials by Gamma-Ray Spectrometry. *J. Radiation Protection Dosimetry*, 138 (3), 264–277. doi:10.1093/rpd/ncp239.

13 Ramebäck, H., Vesterlund, A., Tovedal, A., Nygren, U., Wallberg, L., Holm, E., Ekberg, C., Skarnemark, G. (2010): "The Jackknife as an Approach for Uncertainty Assessment in Gamma Spectrometric Measurements of Uranium Isotope Ratios". *Nuclear Instruments and Methods in Physics Research B: Beam Interactions with Materials and Atoms*, 268 (16), 2535–2538.

14 Simpson, J.J., Grün, R. (1998): "Non-Destructive Gamma Spectrometric U-Series Dating". *J. Quaternary Geochronology*, 17, 1009–1022.

15 Yücel, H., Cetiner, M.A. and Demirel, H. (1998): Use of the 1001 keV Peak of 234mPa Daughter of 238U in Measurement of Uranium Concentration by HPGe Gamma-Ray Spectrometry. *Nuclear Instruments and Methods in Physics Research, Section* A, 413, 74–82.

16 Pöllänen, R., Ikäheimonen, T.K., Klemola, S., Vartti, V.P., Vesterbacka, K., Ristonmaa, S., Honkamaa, T., Sipilä, P., Jokelainen, I., Kosunen, A., Zilliacus, R., Kettunen, M., Hokkanen, M. (2003): "Characterization of Projectiles Composed of Depleted Uranium". *J. Environmental Radioactivity*. 64, 133–142.

17 UNSCEAR (2000): United Nations Scientific Committee on the Effects of Atomic Radiation, ''Sources and Effects of Ionizing Radiation''. Report to General Assembly, with Scientific Annexes United Nations. United Nations, New York.

18 Weyer S., Anbar A. D., Gerdes A., Gordon G. W., Algeo T. J. and Boyle E. A. (2008): Natural fractionation of 238U/235U. *J. Geochim. Cosmochim. Acta*, 72, 345–359.

19 Montoya-Pino, C., Weyer, S., Anbar, A. D., Pross, J., Oschmann, W., Schootbrugge, B., Arz, H. W. (2010): Global enhancement of ocean anoxia during Oceanic Anoxic Event 2: A quantitative approach using U isotopes. Geology, 38, 315–318.

20 Bigeleisen, J. (1996): "Nuclear Size and Shape Effects in Chemical Reactions; Isotope Chemistry of the Heavy Elements". *J. Am. Chem. Soc*., 118, 3676–3680.

21 Schauble, E.A. (2007): Role of nuclear volume in driving equilibrium stable isotope fractionation of mercury, thallium, and other very heavy elements. *J. Geochim. Cosmochim. Acta*, 71, 2170– 2189.

22 Min, M. - Z., Luo, X. - Z., Du, G.S., He, B. – A. and Campbell, A.R. (1999): Mineralogical and geochemical constraints on the genesis of the granite-hosted Huangao uranium deposit, SE China. *J. Ore Geol. Rev*. 14, 105-127.

23 El Aassy, I. E., El Feky, M. G., El Kasaby, M. A., Ibrahim, E. M., Sewefi, S. S., Attia, R. M. (2017): Behavior of Radionuclides during Acidic Leaching Processes of Different Rock Materials, Allouga Locality, Southwestern Sinai, Egypt. International *J. Scientific & Engineering Research*, 8, (1), 1135-1147.

24 Rudnick, R. L. and Gao, S. (2004): Composition

of the Continental Crust. In: Treatise on Geochemistry. Holland, H.D. and Turekian, K.K. (Editors), Elsevier, Amsterdam. 3: 1-64.

25 El-Mezayen, A. M., El-Feky, M. G., Omar, S. A. and Ibrahim, S. A. (2015): Geochemistry and a composite M-type with W-type of REE tetrad effect in altered granites of Abu Furad area, Central Eastern Desert, Egypt. Greener. *J. Geology and Earth Sciences*, 3 (2), 013-029.

26 El Kholy, D. M., Khamis, H. A. and El Sandouly, H. L. (2017): Geology and Structural relationship Between Uranium Occurrences in the Northern Part of Gabal Gattar, Northern Eastern Desert, Egypt. *J. Nuclear Materials Authority*, 7, 64-84.

27 Taylor, S. R. and McLennan, S. M. (1985): The Continental Crust; Its composition and evolution; an examination of the geochemical record preserved in sedimentary rocks. Blackwell, Oxford, 312.

28 Irber, W. (1999): The lanthanide tetrad effect and its correlation with K/Rb, Eu/Eu*, Sr/Eu, Y/Ho, and Zr/Hf of evolving peraluminous granite suites. *J. Geochim. Cosmochim. Acta*. 63, 489–508.